JOURNAL OF MATERIALS SCIENCE 29 (1994) 1983–1990

The interface in Al_2O_3 particulate-reinforced aluminium alloy composite and its role on the tensile properties

J. C. LEE, K. N. SUBRAMANIAN
Department of Materials Science and Mechanics, Michigan State University. East Lansing, MI 48823, USA

Y. KIM
Ames Laboratory, US DOE, Ames, IA 50011, USA

The interface characterization of the aluminium alloy reinforced with Al_2O_3 particulates ($(Al_2O_3)_p$/Al composite) was performed using X-ray diffractometry and energy dispersive X-ray spectroscopy. A layer of $MgAl_2O_4$ single crystals was observed at the $(Al_2O_3)_p$/Al interface in the as-received extruded composites. Such $MgAl_2O_4$ crystals formed at the surface of $(Al_2O_3)_p$ are believed to grow by consuming a certain amount of $(Al_2O_3)_p$. Upon loading, interfacial debonding was observed to occur at the boundary between $MgAl_2O_4$ and the aluminium alloy, or along the $MgAl_2O_4$ layer itself. These experimental observations are correlated with the tensile properties of such composites.

1. Introduction

Interfacial characteristics can be considered as one of the most important factors in determining the mechanical properties of composites, because a strong interfacial bond is essential for the effective load transfer from matrix to reinforcement to achieve higher strength of the composites. Such a strong bond is usually achieved by the formation of an adequately thin reaction layer at the interface under favourable wetting conditions of the molten matrix on to the reinforcement. However, it has been reported that nearly all commercially important ceramic reinforcements, including SiC, Al_2O_3, B_4C, etc., exhibit poor wettability by a molten matrix [1–6]. Molten pure aluminium does not wet Al_2O_3 even at 900 °C [7, 8]. Addition of alloying elements, such as lithium or magnesium, has proved to be an effective method to enhance the wettability of the ceramic reinforcements by the molten matrix. Some of these alloying elements can react with the reinforcements to produce chemical reaction products at the interface, which might be either beneficial or undesirable for the composite strengthening. For example, the formation of a thick intermetallic compound layer at the interface will cause crack initiation at the interface (i.e. interfacial debonding) upon loading due to the stress concentration at the brittle interface, resulting in low strength and ductility of the composite. In contrast, the interfacial bond can be improved by the formation of spinels, which is believed to promote the bond strength between metals and ceramics [9, 10].

Significant studies, using electron diffraction [7, 11–14], Auger spectroscopy [7, 9], and energy dispersive X-ray spectroscopy (EDS) [9, 12, 14], have been carried out to characterize the structure and the chemistry of the interface in the aluminium alloy composites reinforced with Al_2O_3 fibre. Although the interfacial bond in these composites was found to be achieved by the formation of $MgAl_2O_4$ spinel [7, 9–15], studies to demonstrate the detailed morphology of $MgAl_2O_4$ and the structure of the reaction layer have not yet been reported in the literature. The aim of the present study was to characterize the interfacial reaction layer in $(Al_2O_3)_p$/Al composite, and to investigate its influence on the resultant tensile properties.

2. Experimental procedure

2.1. Material

Cast Duralcan composite (W6A 10A), 6061 aluminium alloy reinforced with 10% $(Al_2O_3)_p$, and obtained as extruded cylindrical bars with a diameter of 2 in, was used for the present study. The composite was T6 heat treated prior to the microstructural studies and tensile testing. Details of the heat-treatment procedures used are as follows:

(a) solution treatment, 560 °C, 1 h;
(b) room-temperature ageing, 24 °C, 65 h;
(c) artificial ageing, 170 °C, 14 h.

2.2. Sample preparation and microstructural studies

The heat-treated specimens were polished with diamond compound on a lapping wheel. The polished surfaces were then etched lightly with dilute Keller's reagent to reveal the outer contours of the interface and the precipitates in the matrix. The interface region

0022–2461

in the polished surfaces and the fracture surface of the fractured tensile test specimens were examined using SEM and EDS. X-ray line scanning across the interface, and X-ray dot mapping of the interfacial region, were performed using EDS operated at 15 kV.

Electrochemical dissolution, with 33% HNO_3–67% methanol, was employed to dissolve away the conductive aluminium matrix along with the precipitates, such as $CuAl_2$, Mg_2Si, etc., present within the matrix. This process helped to obtain the non-conductive phases present at the interface for further study. The crystal structures of these phases were determined by X-ray diffractometry. Because the volume fraction of the reaction product layer at the interface is relatively small compared to that of $(Al_2O_3)_p$, a slow scan speed ($0.4^\circ\ min^{-1}$) was used to obtain sharp and strong enough X-ray diffraction peaks corresponding to the reaction products formed at the interface. (Direct X-ray scanning of the composite surface was not effective for identifying the interfacial reaction products owing to their small volume fraction in the composite.) The detailed morphologies of $(Al_2O_3)_p$ and the reaction products at the interface were examined using SEM.

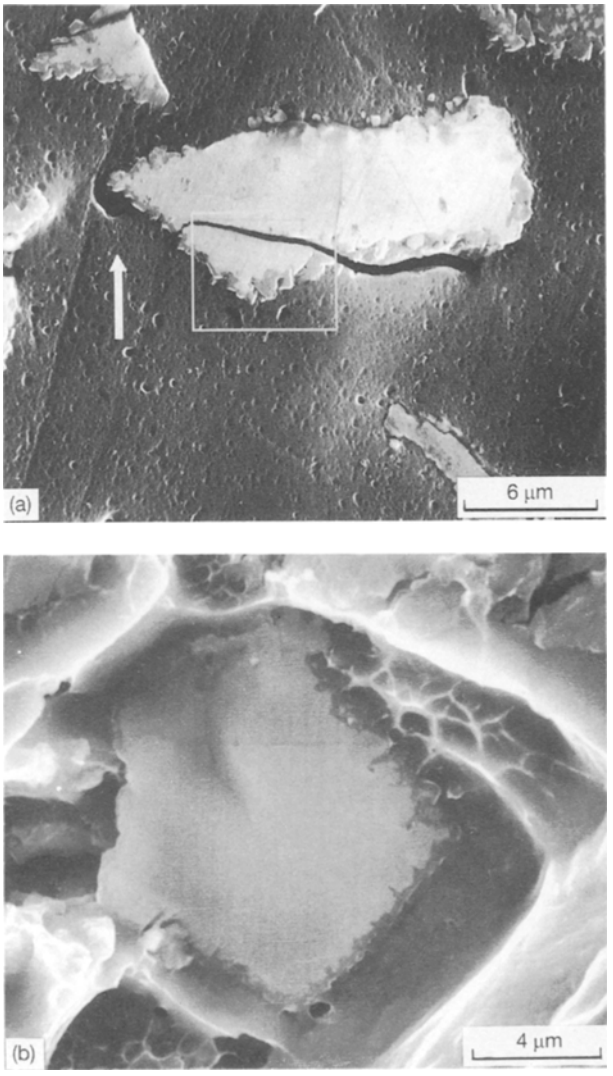

Figure 1 (a) Micrograph taken from the polished surface. The reaction layer at the interface, and some precipitates in the matrix can be seen. The crack inside the region marked by the rectangle is due to the tensile loading applied in a direction indicated by the arrow. Note that the crack formed within the particulate propagates around the reaction layer. (b) Micrograph taken from the fracture surface. The jagged reaction layer is evident at the interface. The smooth fracture surface of $(Al_2O_3)_p$ indicates that $(Al_2O_3)_p$ probably is single crystal.

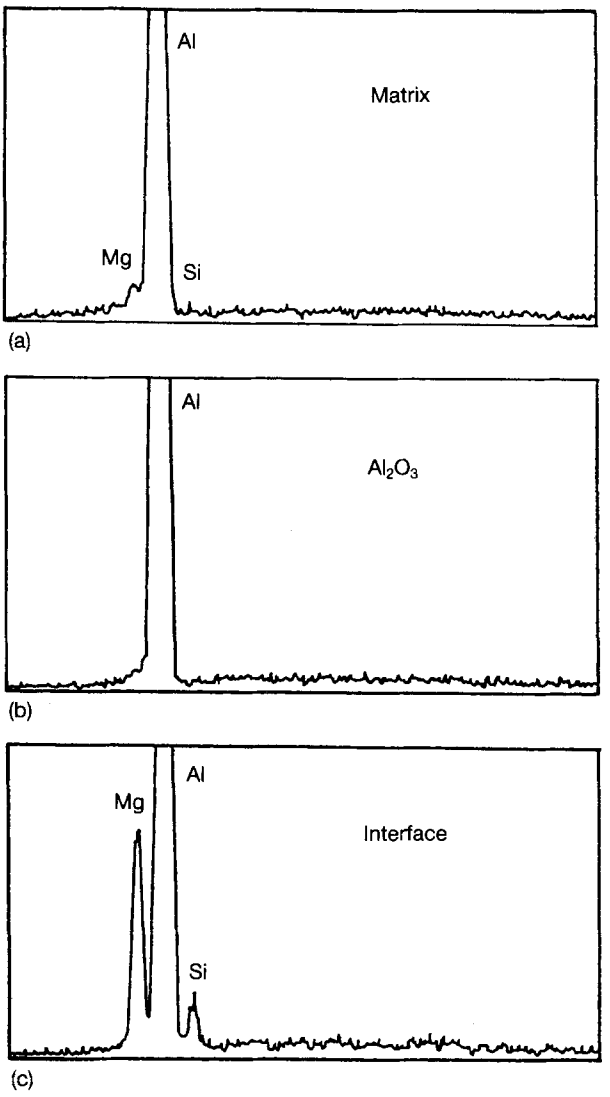

Figure 2 EDS analyses of (a) matrix, (b) $(Al_2O_3)_p$, and (c) interfacial region.

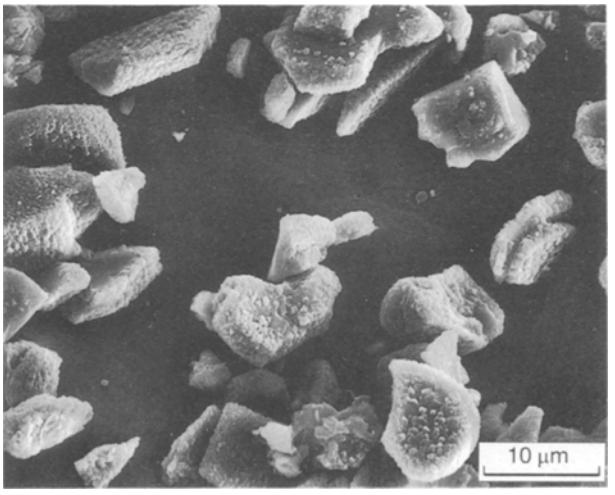

Figure 3 Surface of $(Al_2O_3)_p$/Al composite showing individual $(Al_2O_3)_p$. Most $(Al_2O_3)_p$ are fully, and some partially, covered with small crystals. (Electrolytic polishing was carried out to remove the conductive matrix).

Tensile testing of dog-bone type specimens, cut out from the composite, were carried out using an Instron with a constant crosshead speed (1 cm min^{-1}) at room temperature. The fracture surfaces, and side surfaces of the fractured tensile test specimens were examined using SEM to understand the fracture behaviour exhibited by such composites. Observations made on the fracture surfaces of the tensile tested specimens, and on the surfaces of electropolished composite scratched with a metal scriber, helped to identify the phase boundary where interfacial debonding occurred.

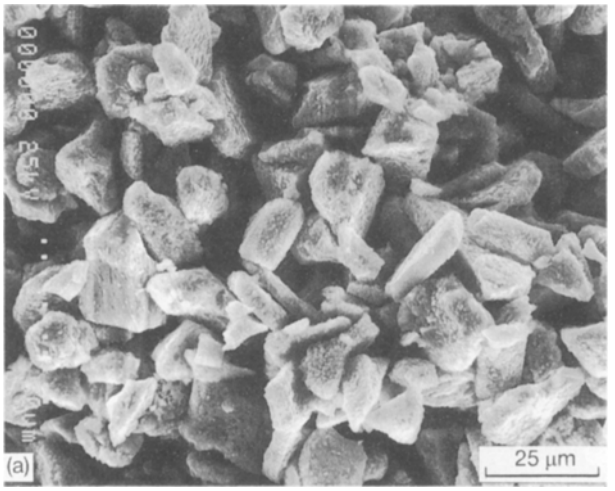

3. Results and discussion

3.1. Interface characterization

The SEM image obtained from the polished surface, Fig. 1a, clearly shows the interfacial reaction layer as well as the precipitates in the matrix. Such a reaction layer can also be observed from the fracture surfaces of the tensile test specimens, as shown in Fig. 1b. The jagged shape of the interface region can be seen clearly from both these micrographs. EDS analyses employed on this interfacial region (Fig. 2) shows a relatively strong magnesium peak as well as a noticeably weak silicon peak, indicating that the interfacial reaction products consist of magnesium and silicon.

Electrolytic polishing of the specimens, carried out to reveal the individual $(Al_2O_3)_p$ showed the detailed

Figure 4 (a) Al_2O_3 particles covered with small crystals were obtained using electrochemical dissolution for XRD. (b) XRD peaks indicate that the type of the reinforcement is α-Al_2O_3 and the crystals formed at the surface of Al_2O_3 are spinel ($MgAl_2O_4$).

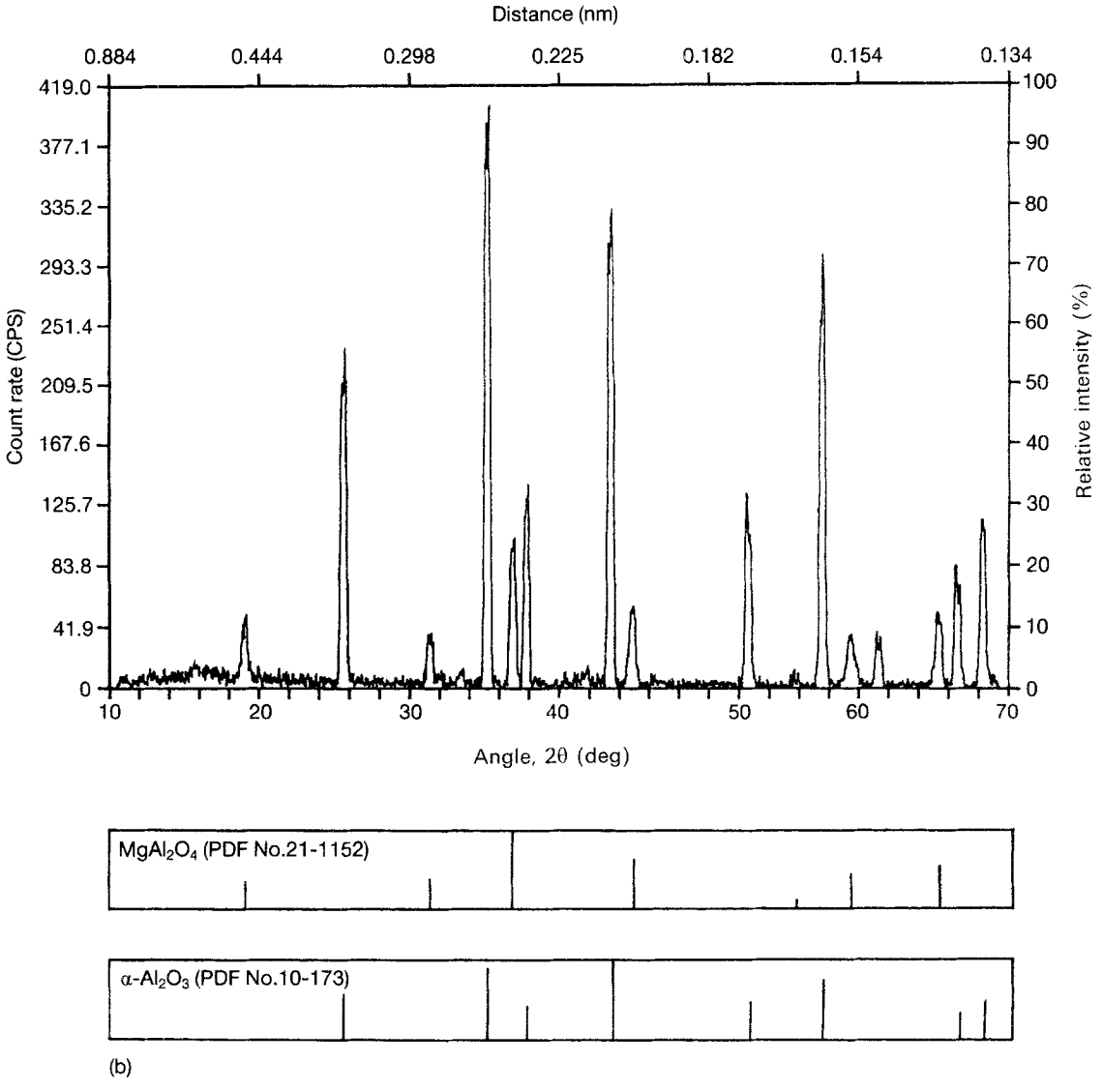

shape of $(Al_2O_3)_p$. These $(Al_2O_3)_p$ have a blocky platelet shape with an aspect ratio of about 2, and are either fully or partially covered with small crystals, as shown in Fig. 3. The results obtained from the X-ray diffractometry (Fig. 4) show that the type of $(Al_2O_3)_p$ is α-Al_2O_3 having corundum structure, and the small crystals formed at the surface of $(Al_2O_3)_p$ are $MgAl_2O_4$ with spinel structure. As can be seen in the magnified views of individual $(Al_2O_3)_p$ given in Figs 5 and 6, $MgAl_2O_4$ formed at the surface of $(Al_2O_3)_p$ are pyramid-like (or octahedral-shaped) crystals with an average size of about 1 μm. Based on the shape of these individual $MgAl_2O_4$ spinel regions, they are believed to be single crystals. The micrographs also reveal that the roots of $MgAl_2O_4$ are located well below the surface of $(Al_2O_3)_p$. Furthermore, it is noted that the inner surface contour of Al_2O_3, which surrounds each $MgAl_2O_4$ crystal, matches the outer contour of the $MgAl_2O_4$. Such microscopic features, as can be seen in Figs 5a and 6, indicate that these crystals might have grown at Al_2O_3 substrates at the expense of some amount of Al_2O_3. Infrequently, however, some $MgAl_2O_4$ crystals have been found in the matrix near $(Al_2O_3)_p$, as shown in Fig. 7. Such a

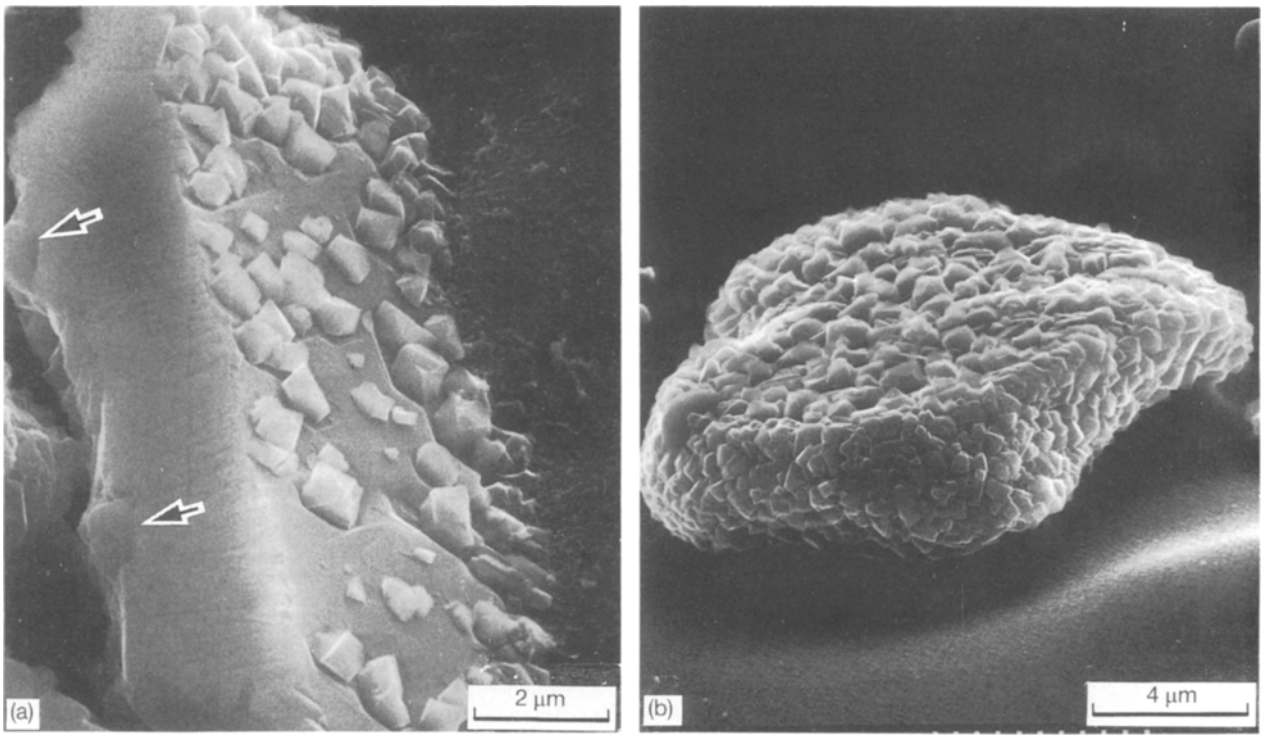

Figure 5 (a) $(Al_2O_3)_p$ partially covered with $MgAl_2O_4$. The roots of the crystals are embedded in Al_2O_3 at locations indicated by the arrows. The flat surface on $(Al_2O_3)_p$ is due to mechanical polishing, and the dark background is the matrix. (b) $(Al_2O_3)_p$ fully covered with $MgAl_2O_4$ crystals.

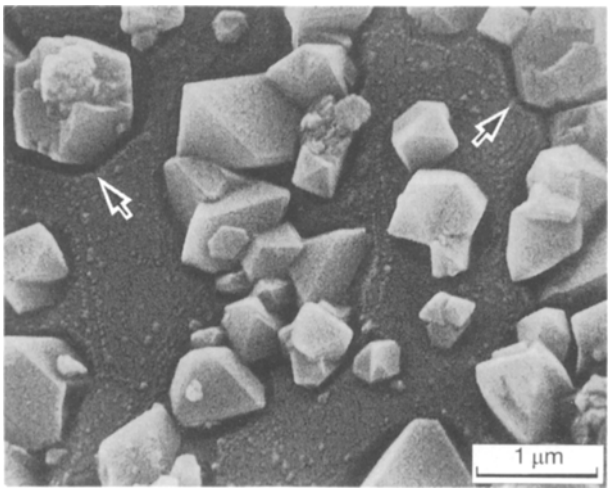

Figure 6 $MgAl_2O_4$ single crystals, grown at the surface of $(Al_2O_3)_p$, observed at a higher magnification (×20 000). Notice the groove around individual $MgAl_2O_4$ crystals at regions indicated by the arrows. The flat dark background is the surface of $(Al_2O_3)_p$.

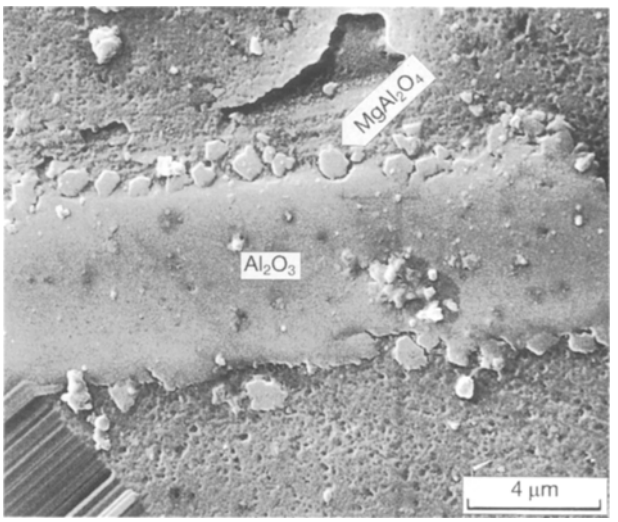

Figure 7 $MgAl_2O_4$ crystals infrequently formed in the vicinity of $(Al_2O_3)_p$. Note that $MgAl_2O_4$ crystals, similar to that indicated in the figure, are not in contact with $(Al_2O_3)_p$.

microscopic feature indicates a strong interfacial bond between $MgAl_2O_4$ (spinel) and Al_2O_3 (corundum). The fracture surfaces of $(Al_2O_3)_p$ reveal the well-bonded interface between Al_2O_3 and $MgAl_2O_4$ (Fig. 8).

A fairly thick $MgAl_2O_4$ layer, about 1 μm, observed at the interfacial region is probably due to prolonged contact between $(Al_2O_3)_p$ and molten aluminium during manufacture of the composite. X-ray dot mapping (Fig. 9a) and line scanning across the interface (Fig. 9b, c) were carried out on $(Al_2O_3)_p$/Al composite using EDS in this study. The strong X-ray signal indicating the presence of magnesium near the interface observable in Fig. 9a, is due to the $MgAl_2O_4$ layer.

Silicon has been reported to be present either in the form of Mg_2Si precipitates near the interface, or as a silicon-rich amorphous layer, in these composites [11–14, 16]. The presence of silicon at the interfacial region could not be clearly noted from the results obtained using elemental X-ray dot mapping (owing to its slightly higher contribution as compared to the matrix) as shown in Fig. 9a. However, the corresponding line scanning pattern across the interface shows the presence of a small amount of silicon at the interface region, as shown in Figs 2 and 9b, c. The techniques employed in this study could not characterize the silicon-containing phase, segregated at the interface.

3.2. Formation of the interfacial products

Based on thermodynamic considerations, the following reactions have been suggested for the formation of the $MgAl_2O_4$ at the $(Al_2O_3)_p$/Al interface in this type of composite [9, 11, 12, 15]

$$\{Mg\} + 2\{Al\} + 2\{O_2\} = [MgAl_2O_4] \quad (1)$$

$$[MgO] + [Al_2O_3] = [MgAl_2O_4] \quad (2)$$

$$\{Mg\} + \tfrac{4}{3}[Al_2O_3] = [MgAl_2O_4] + \tfrac{2}{3}\{Al\} \quad (3)$$

$$2[SiO_2] + 2\{Al\} + \{Mg\} = [MgAl_2O_4] + 2\{Si\} \quad (4)$$

where { } and [ ] in above equations correspond to those in solution in the melt and those present as solid phase in the melt, respectively. All of the reactions

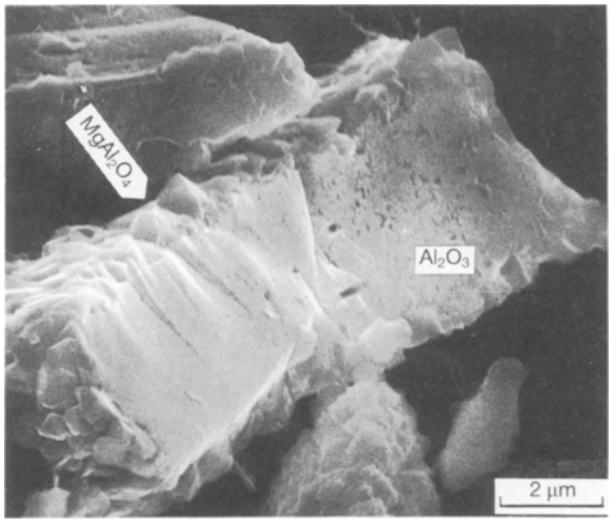

Figure 8 The river patterns extending from $MgAl_2O_4$ to Al_2O_3 on the fracture surface of $(Al_2O_3)_p$ illustrate the existence of a well-bonded interface between Al_2O_3 and $MgAl_2O_4$.

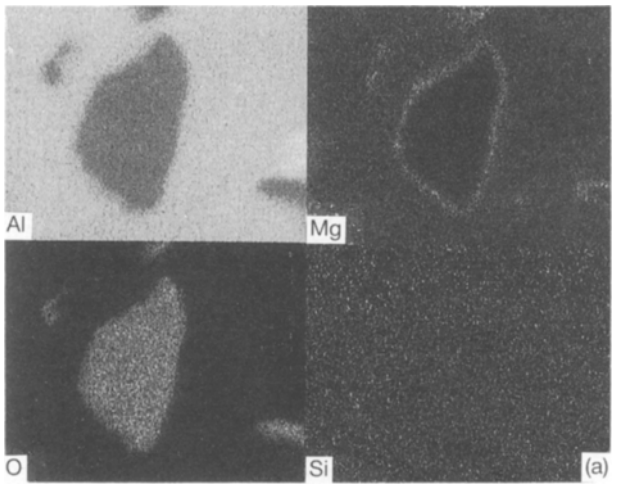

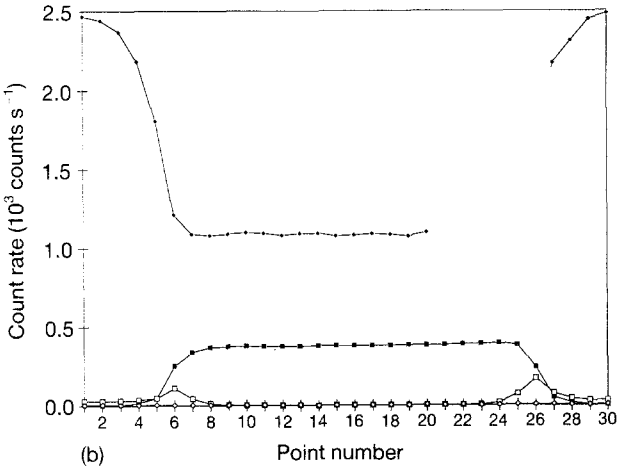

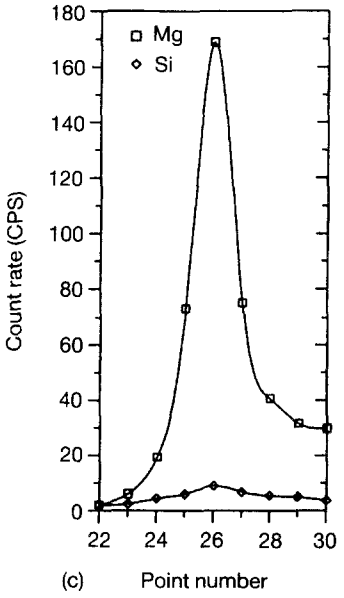

Figure 9 (a) Elemental X-ray dot maps obtained from the particulate and interfacial region. The presence of silicon at the interfacial region is not clear because the concentration of silicon in this region is only slightly higher than that in the matrix. (b, c) EDS line scans for (◆) aluminium, (■) oxygen (□) magnesium and (◇) silicon across the interface. Line scans was carried out for 30 different points at intervals of 0.375 μm.

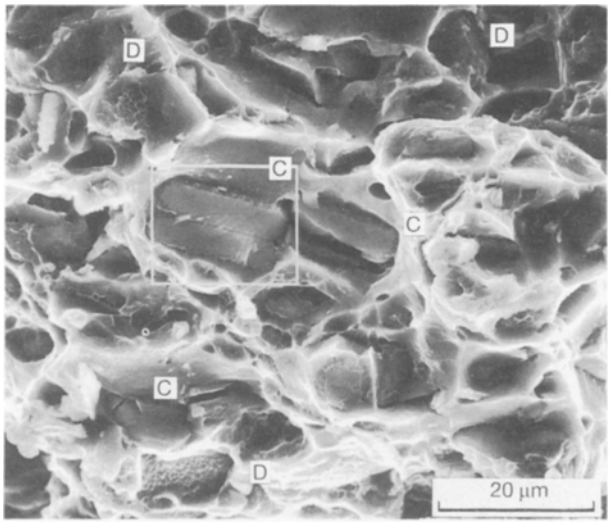

Figure 10 Fracture surface of T6 heat-treated $(Al_2O_3)_p$/Al composite showing the particulate cracking, C, and interfacial debonding, D. Limited plastic deformation of the matrix can also be seen. The fracture strain of the specimen was about 7%.

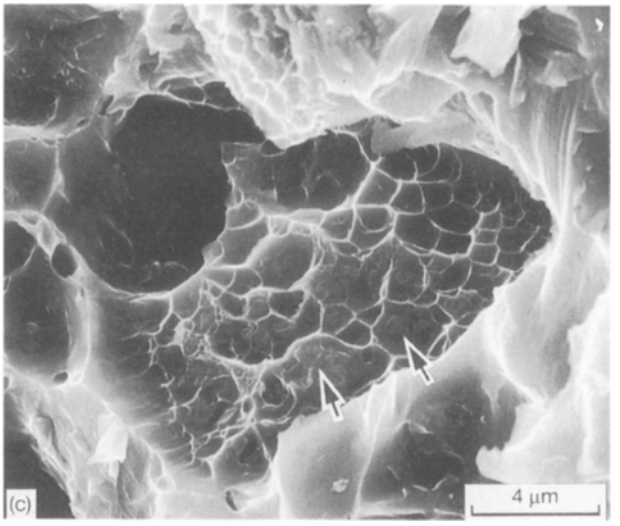

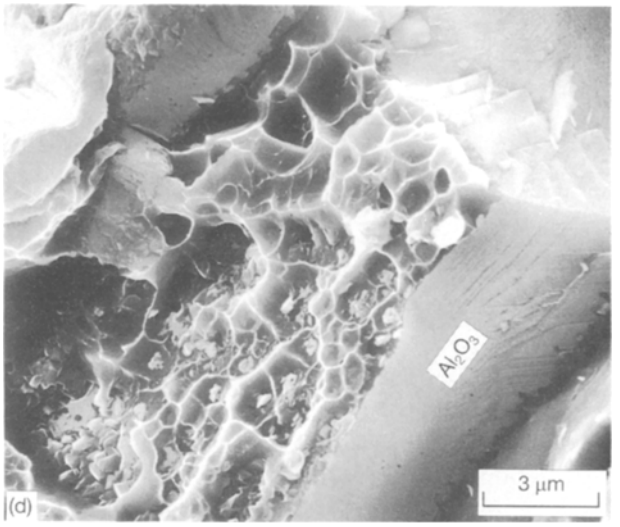

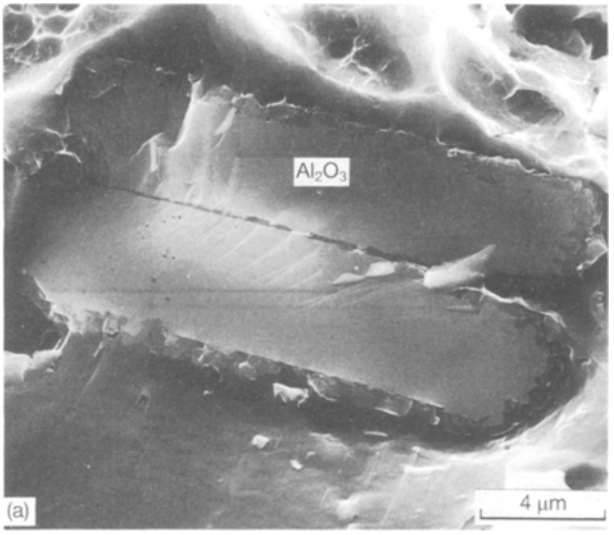

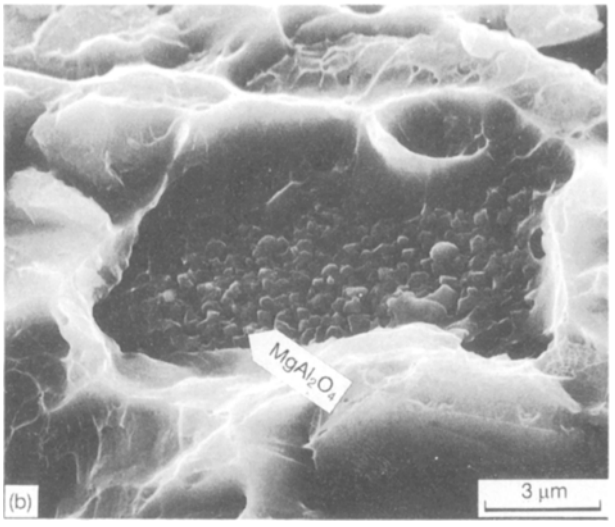

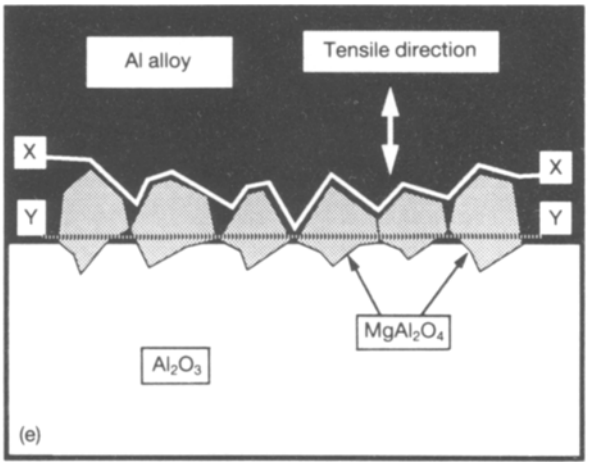

Figure 11 (a) Fracture surface of $(Al_2O_3)_p$ with the reaction layer around it. Note that the surface of $(Al_2O_3)_p$ at the interface region is relatively straight, indicating that $MgAl_2O_4$ crystals in this region are not grown at the expense of $(Al_2O_3)_p$. Such cases were noticed infrequently. (b) Outer surface of $(Al_2O_3)_p$ covered with $MgAl_2O_4$ crystal layer, indicating interfacial debonding along the $MgAl_2O_4$/Al phase boundary. (c) Matrix region from which $MgAl_2O_4$ layer is debonded. A few $MgAl_2O_4$ crystals stuck to the matrix can be noted at the regions indicated by the arrows. (d) Outer surface of $(Al_2O_3)_p$ when interfacial debonding occurs at the $MgAl_2O_4$ layer itself. The roots of $MgAl_2O_4$ can be observed from the sub-surface of $(Al_2O_3)_p$. (e) Schematic illustration of interfacial debonding: Line XX represents interfacial debonding along the $MgAl_2O_4$/Al phase boundary corresponding to micrographs given in (b) and (c). Line YY represents interfacial debonding along the $MgAl_2O_4$ layer itself corresponding to micrograph given in (d).

listed above have large enough thermodynamic driving forces for the formation of $MgAl_2O_4$ spinel.

Although both the phase boundary and the grain-boundary regions provide heterogeneous nucleation sites, most of the $MgAl_2O_4$ crystals were found to be present mainly at the $(Al_2O_3)_p$/Al phase boundary. Based on this observation, Reaction 1 seems to be less likely. Reaction 2 has to occur as a solid-state reaction between two ceramic materials, which kinetically will be very slow [9].

The micrographs given in Figs 5a and 6, indicate that $MgAl_2O_4$ crystals usually have their roots embedded in $(Al_2O_3)_p$ and appear to have been formed by consuming some amount of Al_2O_3. The presence of grooves around the $MgAl_2O_4$ crystals, existing at the surface of $(Al_2O_3)_p$ obtained by electrochemical dissolution, may correspond to pure aluminium resulting from this reaction that has been dissolved during electrochemical dissolution. Such observations tend to favour Reaction 3.

However, Reaction 4, which describes the formation of $MgAl_2O_4$ in the absence of Al_2O_3 substrate, is a possible mechanism that can explain the observed presence of magnesium and silicon near the interface. The presence of some $MgAl_2O_4$ crystals in the matrix region near the interface, as shown in Fig. 7 may be due to Reaction 4. The source of SiO_2 required for this reaction may arise from silicon and oxygen present in the molten aluminium.

On the basis of the microscopic observation, Reaction 3 is believed to be the most likely mechanism for the formation of the $MgAl_2O_4$ layer at the interface, because the features supporting it have been observed much more frequently than those supporting Reaction 4.

3.3. Role of the interface on the tensile properties

Several studies have been carried out to investigate the failure behaviour of metal matrix composites reinforced with ceramic particulates [17–19]. Based on these studies, the low ductility exhibited by such composites can be attributed to "particulate cracking" and "interfacial debonding" that occur upon loading. A typical fracture surface of $(Al_2O_3)_p$/Al composite showing these significant microscopic features is given in Fig. 10.

Particulate cracking (Fig. 11a), which acts as a dominant failure mechanism operative in this composite, occurs as a result of the stress concentration at $(Al_2O_3)_p$ under the applied tension [19]. The jagged edges of $(Al_2O_3)_p$, produced as a result of the severe interfacial reaction, will cause stress concentration and aid particulate cracking.

In addition to particulate cracking, a significant amount of interfacial debonding could be observed at the side surfaces of the fractured tensile test specimens. Because a distinct $MgAl_2O_4$ layer, with a thickness of about 1 μm was found to be present at the $(Al_2O_3)_p$/Al interface, interfacial debonding can occur either at (i) the $(Al_2O_3)_p/MgAl_2O_4$ phase boundary, (ii) the $MgAl_2O_4$/Al phase boundary, or (iii) the $MgAl_2O_4$ layer itself (by fracturing individual crystals). Of these, the first one has never been observed during the course of this study, indicating a strong interfacial bond between $(Al_2O_3)_p$ and $MgAl_2O_4$. Interfacial debonding at the $MgAl_2O_4$/Al phase boundary, as illustrated in Fig. 11b and c, was frequently observed. Debonding resulting from the fracture of $MgAl_2O_4$ crystals present in the interfacial reaction layer (Fig. 11d), was noticed less frequently. These results are schematically illustrated in Fig. 11e. Further evidence of the above observations was also obtained by scratching the electropolished surface of the composite with a metal scriber. Such a procedure was found to pull out $(Al_2O_3)_p$ along with $MgAl_2O_4$ crystals, leaving the dimple-like matching region (corresponding to $MgAl_2O_4$ crystals that have been pulled out) in the matrix. This matrix region, from which $(Al_2O_3)_p$ is pulled out, is usually devoid of $MgAl_2O_4$, as can be observed in the micrograph given in Fig. 12.

The strength and ductility of $(Al_2O_3)_p$/Al composites are considerably lower than those of SiC_p/Al composites having the same volume fraction of reinforcements [20–23], although mechanical properties of SiC_p and $(Al_2O_3)_p$ reinforcements are similar to each other [24, 25]. Slight differences in thermal history, morphology and size of the reinforcements cannot provide sufficient reasoning for the observed differences. In SiC_p/Al composites, particulate cracking has been found to be more predominant than interfacial debonding [13, 19]. However, in $(Al_2O_3)_p$/Al composite, significant interfacial debonding occurs in addition to particulate cracking. When interfacial debonding occurs, load transfer from the matrix to the reinforcement becomes less effective during further loading. The lower strength and ductility of

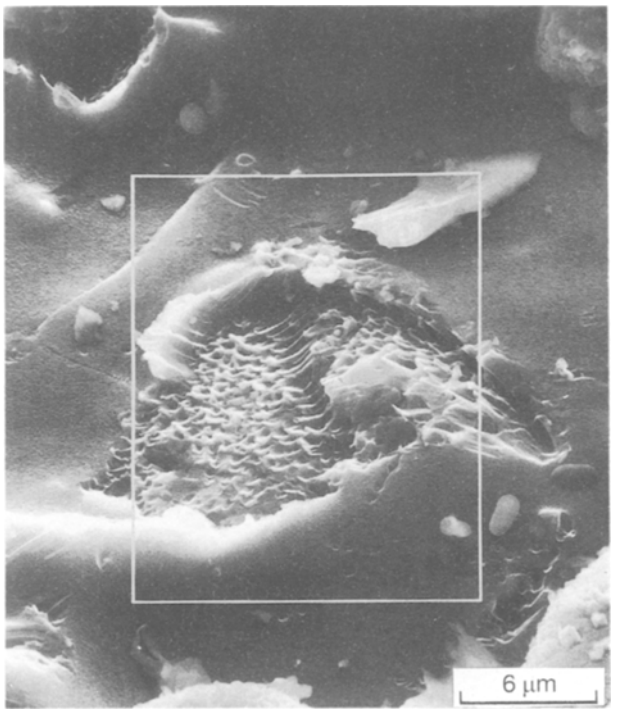

Figure 12 Matrix region from which $(Al_2O_3)_p$ is pulled out by scratching the surface of the electropolished composite. The dimples are due to the interfacial debonding between the aluminium alloy and $MgAl_2O_4$ layer.

$(Al_2O_3)_p$/Al composites, compared to SiC_p/Al composite, can be explained on the basis of less-effective load transfer due to interfacial debonding.

4. Conclusion

4.1. Characterization of the interface

The chemical reaction products found to exist at the interface of $(Al_2O_3)_p$/Al composites consist of a layer containing single crystals of $MgAl_2O_4$ spinel. Each $(Al_2O_3)_p$ is fully (or almost fully) covered with $MgAl_2O_4$ single crystals, about 1μm in size. Based on the microstructural and thermodynamic considerations, each $MgAl_2O_4$ single crystal is believed to have grown at the surface of $(Al_2O_3)_p$ by the reaction between $(Al_2O_3)_p$ and magnesium in the molten matrix segregated at the interface region. The reaction between SiO_2 and molten matrix, however, is believed to be a less significant reaction for the formation of $MgAl_2O_4$ crystals observed in the interface region.

4.2. Role of the interface on the tensile properties

Observations on the side surfaces of the fractured tensile specimens of $(Al_2O_3)_p$/Al composite have shown that interfacial debonding as well as particulate cracking play significant roles in the fracture of this composite. Among the various possibilities, interfacial debonding owing to the fracture along $MgAl_2O_4$/Al phase boundary was found to occur more frequently than that due to the cracking of the $MgAl_2O_4$ layer. Significant interfacial debonding that occurs in $(Al_2O_3)_p$/Al composites during tensile loading can be the contributing factor to their inferior tensile properties compared to those of SiC_p/Al composites.

Acknowledgements

The authors thank Mr Stephen Holcomb, Duralcan Co., for providing the materials used in this study, and also Mr J. M. Yoo and Mr S. Nam, Michigan State University, for their assistances during this research.

References

1. F. M. HOSKING, F. F. PORTILLO, R. WUNDERLIN and R. MEHRABIAN, *J. Mater. Sci.* **17** (1982) 477.
2. S. DEONATH, R. BHATT and P. ROHATGI, *ibid.* **15**, (1980) 1241.
3. B. C. PAI, S. PAY, K. V. PRABHAKAR and P. K. ROHATGI, *Mater. Sci. Eng.* **24** (1976) 31.
4. P. K. ROHATGI, B. C. PAI and S. C. PANDA, *J. Mater. Sci.* **14** (1979) 2277.
5. M. K. SURRPA and P. K. ROHATGI, *ibid.* **16** (1981) 983.
6. T. W. CLYNE, M. G. BADER, G. R. CAPPLEMAN and P. A. HUBERT, *ibid.* **20** (1985) 85.
7. A. MUNITZ, M. METZGER and R. MEHRABIAN, *Metall. Trans.* **10A** (1979) 1491.
8. R. E. TRESSLER, in "Composite Material", Vol. 1 Interface in metal matrix composites, edited by A. G. Metcalfe (Academic Press, New York, London, 1974) pp. 296.
9. C. G. LEVI, G. J. ABBASCHIAN and R. MEHRABIAN, *Metall. Trans.* **9A** (1978) 697.
10. P. K. ROHATGI, *J. Metals* **43** (4) (1991) 10.
11. B. HALLSTEDT, Z. K. LIU and J. ARGEN, *Mater. Sci. Eng.* **129A** (1990) 135.
12. R. MOLINS, J. D. BARTOUT and Y. BIENVENU, *ibid.* **135A** (1991) 111.
13. G. M. JANOWSKI and B. J. PLETKA, *ibid* **129A** (1990) 65.
14. H. HINO, M. KOMATSU, Y. HIRASAWA and M. SASAKI in "Proceedings of the Fifth Annual ASM/EDS Advanced Composites Conference", Detroit, Michigan, October 1989, (ASM International, Materials Park, OH, 1989) pp. 201–8.
15. B. F. QUIGLEY, G. J. ABBASCHIAN, R. WUNDERLIN, and R. MEHRABIAN, *Metall. Trans.* **13A** (1982) 93.
16. J. P. LUCAS, J. J. STEPHENS and F. A. GREULICH, *Mater. Sci. Eng.* **131A** (1990) 221.
17. S. R. NUTT and J. M. DUVA, *Scripta Metall. Mater.* **20** (1986) 1055.
18. T. CHRISTMAN, A. NEEDLEMAN, S. R. NUTT and S. SURESH *Mater. Sci. Eng.* **107A** (1989) 49.
19. J. C. LEE and K. N. SUBRAMINIAN, *J. Mater. Sci.*, **27** (1992) 5453.
20. T. G. NIEH and D. J. CHELLMAN, *Scripta Metall. Mater.* **18** (1984) 925.
21. DWA Composite Specialities, Inc., *Light Metal Age* (6) (1986) 7.
22. W. A. HOOVER, in "Proceedings of the Fifth Annual ASM/EDS Advanced Composites Conference", Detroit, Michigan, October 1989, (ASM International, Materials Park, OH, 1989) pp. 211–17.
23. W. C. HARRIGAN Jr, GAEBLER, E. DAVIS and E. J. LEVIN, "Proceedings of a symposium sponsored by the Composite Materials Committee of the Metallurgical Society of AIME and the Materials Science Division of American Society for Metals", 111th AIME Annual Meeting, Dallas, TX, 1982 (Metallurgical Society of AIME, Warrendale, PA, 1983) pp. 169–80.
24. F. A. GIROT, J. M. QUENISSET and R. NASLAIN, *Compos. Sci. Technol.* **30** (1987) 155.
25. D. W. RICHERSON, "Modern ceramic engineering; properties, processing, and use in design" (Marcell Dekker, New York, 1982).

Received 22 May 1992
and accepted 5 March 1993